Cooperative confinement and parametric resonance of multi-species ions in a linear paul trap*

WANG Fei[1], QIAN Jingyu[2], YIN Weibo[2], WANG Yuhan[2], LIANG Weichen[2], JIA Fengdong[2], XUE Ping[1,*], ZHONG Zhiping[2,*]

1. State Key Laboratory of Low-Dimensional Quantum Physics, Department of Physics, Tsinghua University, Beijing 100084, China
2. School of Physical Sciences, University of Chinese Academy of Sciences, Beijing 100049, China

Abstract Trapped ion systems are pivotal for quantum information processing, simulation, and precision measurement. The manipulation of multi-species ion mixtures is not only crucial for advancing quantum technologies but also for fundamental research in plasma physics. However, existing theoretical models, often based on single-species or weakly coupled approximations, cannot accurately describe the complex collective dynamics of strongly coupled multi-species systems. This work aims to investigate these collective effects experimentally, specifically exploring cooperative confinement in multi-species rubidium ion clusters and developing a highly selective ion manipulation method via parametric resonance.

An advanced ion-atom hybrid trap system was employed, integrating a rubidium magneto-optical trap (MOT) and a linear Paul trap. Laser-cooled ^{87}Rb atoms were continuously photoionized to generate multi-species ion clusters $^{87}Rb_N^+$ (N = 1, 2, • • •), whose mass-to-charge ratios form an arithmetic sequence. The ion dynamics were characterized by scanning the frequency (Ω_{RF}) and amplitude (U_{RF}) of the confining radio-frequency field and monitoring the corresponding time-of-flight mass spectra. The radial Mathieu stability parameter q_x serves as the key analysis quantity.

The principal findings are as follows. First, we observed that $^{87}Rb^+$ ions remain stably trapped at $q_x > 0.908$, significantly surpassing the theoretical stability boundary ($q_x < 0.908$) for a single species. A lifetime analysis yielded a lower bound of $\geqslant$1.3 s for these atomic ions under such conditions, far exceeding the characteristic decay

---

* The paper is an English translated version of the original Chinese paper published in Acta Physica Sinica. Please cite the paper as: **WANG Fei, QIAN Jingyu, YIN Weibo, WANG Yuhan[2], LIANG Weichen, JIA Fengdong, XUE Ping, ZHONG Zhiping, Cooperative confinement and parametric resonance of multi-species ions in a linear paul trap.** *Acta Phys. Sin.*, 2026, 75(7): 070301. DOI: 10.7498/aps.75.20251381

time of molecular ions (~0.34 s). This extended stability is attributed to a cooperative confinement effect arising from the collective Coulomb interactions among ions whose secular frequencies form a subharmonic sequence ($\approx 1:1/2:1/3:\cdots$). Second, within this extended stable region, the total ion signal exhibited two sharp minima near $q_x(^{87}\mathrm{Rb}^+) \approx \sqrt{2}$. Mass-resolved analysis confirmed the selective loss of $^{87}\mathrm{Rb}^+$ atomic ions at these points. This phenomenon is identified as a parametric resonance directly excited by the trapping RF field ($\Omega_{\mathrm{RF}} \approx 2\omega_r$), with the dual-minimum structure presumably induced by trap nonlinearities and coupling to higher-order motional modes (e.g., $2\omega_r \pm \omega_z$). Finally, the measured resonance linewidths (2.2 – 4.1 kHz in frequency, 2.5 V in amplitude) demonstrate the high selectivity of this resonant ejection method.

In conclusion, this work experimentally clarifies the dominant role of collective interactions in the dynamics of strongly coupled multi-species ion systems. The discovery of the cooperative confinement effect expands the effective operational parameter space of ion traps, while the direct excitation of parametric resonance by the trapping field provides a novel, high-selectivity pathway for targeted ion removal. These results advance the understanding of multi-component Coulomb systems and open new avenues for applications in quantum technology and laboratory plasma physics. Future work will involve molecular dynamics simulations to quantitatively model the cooperative confinement mechanism.

Keywords ion-atom hybrid trap; rubidium ion clusters; Mathieu parameter; ion time-of-flight mass spectrometry; parametric resonance

doi: 10.7498/aps.75.20251381
cstr: 32037.14.aps.75.20251381

1 Introduction

Trapped ion systems in ion traps serve as ideal platforms for quantum information processing, quantum simulation, and precision measurement. In recent years, multi-component ion systems have developed rapidly. By introducing cooperative manipulation and interactions between heterogeneous ions, these systems have significantly expanded the physical scope and technical capabilities of the platform, giving rise to a series of cutting-edge interdisciplinary applications. In quantum information science, such systems have enabled quantum logic spectroscopy and sympathetic cooling, making precise studies of ions that cannot be directly laser-cooled or detected possible. In astrophysics and laboratory plasma research, these systems provide a unique experimental window for simulating complex Coulomb crystals inside compact celestial bodies and the transport properties of multi-component

plasmas [1-3].

Quantum logic spectroscopy is a key measurement technique in such systems. Its core principle involves co-trapping an atomic ion (serving as the "logic ion" or "sensor ion") and the target object of study (the "spectroscopy ion") within the same potential well. This technique features two typical application modes. First, the logic ion acts as a quantum sensor to indirectly achieve precise readout and manipulation of the internal quantum states of the spectroscopy ion. Second, the sensor ion serves as a precisely calibrated field strength probe. By monitoring the frequency shift of its internal state, one can infer the strength of perturbation fields in the trap. Comparing and compensating for these perturbations using the response of the spectroscopy ion provides in situ diagnosis and correction schemes for systems such as optical clocks, without requiring external calibration [4-6]. These capabilities make quantum logic spectroscopy an important tool in quantum science, molecular physics, ion-neutral chemical reaction dynamics, and precision measurement [7-11].

Sympathetic cooling is another fundamental technique. It refers to the process where ions that cannot be directly laser-cooled or detected achieve cooling through interaction with a species of ions that can be laser-cooled [12-15]. Together with quantum logic spectroscopy, this technique constitutes the core capability of multi-component ion systems. The effective implementation of both relies on the precise cooperative manipulation of different ion species as a key prerequisite. Currently, related research is mainly based on two-component ion systems, while exploration of broader multi-component systems remains to be deepened. Extending to multi-component scenarios is expected to break through the capability boundaries of existing technologies and open new paradigms for the precise detection of complex ion systems.

In the fields of plasma physics and astrophysics, Coulomb crystals widely exist in systems ranging from laboratory dusty plasmas to the crusts of neutron stars and the cores of white dwarfs. Current research is gradually shifting from ideal single-component or binary models to multi-component plasma systems that better reflect realistic complexity, such as the multi-component ion systems with broad charge distributions found in X-ray burst ashes. Research on such systems is not only a frontier direction in strongly coupled plasma physics but also constitutes a key bridge connecting microscopic physics with macroscopic astronomical phenomena. By trapping and cooling different types of ions in ion traps, highly controllable multi-component ion Coulomb crystals can be constructed at the microscopic scale to simulate physical conditions in astrophysical environments. This clean model provides a critical experimental platform for directly verifying theoretical frameworks and numerical simulations of multi-component Coulomb plasmas. The related results are of significant value for modeling the evolution of compact stars and diagnosing laboratory plasmas[16-18].

Although multi-component ion systems demonstrate unique advantages in quantum information and precision measurement, they also bring challenges in certain high-precision experiments. For instance, in experiments such as ion optical clocks, the presence of trace impurity ions can significantly affect the performance of target ions[19]. Therefore, how to achieve selective manipulation and precise removal of specific ions while maintaining the advantages of multi-component systems has become a key scientific issue in ion trap research. In this context, selective ion removal technology plays an irreplaceable role in maintaining the purity of quantum systems and improving the precision of spectral detection [20-22].

When multiple ions coexist in an ion trap, their Coulomb coupling induces complex collective dynamical behaviors. However, existing theoretical models are mostly based on single-component or weak-coupling approximations, making it difficult to accurately describe the actual physical picture in multi-component scenarios. In recent years, experimental studies have observed the phenomenon of radial macro-motion frequencies moving closer to each other due to coupling in $^{40}Ca^{+}$-$^{9}Be^{+}$ two-component Coulomb crystals[23], indicating that coupling effects cannot be ignored. Nevertheless, systematic experimental research on the collective dynamical behaviors of multi-component ion systems composed of more ion species is still lacking.

This study is based on an ion-atom hybrid trap experimental platform. We prepared rubidium ion clusters ($^{87}Rb_N^+$ $(N = 1,2,\cdots)$) with mass-to-charge ratios distributed in an arithmetic progression by continuously photoionizing cold ^{87}Rb atoms in a magneto-optical trap. By scanning the frequency and amplitude of the trapping radio-frequency field separately and measuring using time-of-flight mass spectrometry, we investigated the sympathetic trapping characteristics of multi-component ion systems. Furthermore, we explored experimental methods for achieving highly selective ion removal based on parametric resonance.

2 Experimental Methods

The research in this paper is based on an ion-atom hybrid trap platform. The apparatus used was constructed based on the scheme in Reference [24] and is described in detail in Reference [25]. Briefly, the apparatus consists of a standard rubidium atom magneto-optical trap and a linear Paul trap. The geometric centers of the atomic cloud and the ion cloud coincide. The science chamber is a polyhedral, flat, non-magnetic stainless steel chamber with an internal radius of approximately 90 mm and a height of approximately 74 mm. The performance parameters of the magneto-optical trap are as follows: the total number of cold rubidium atoms N_0 is approximately 1×10^8, the density of cold atoms is $(2-4) \times 10^{10}\mathrm{cm}^{-3}$, the $1/e$ radius of the cold atomic cloud is approximately 0.5 mm, and the temperature T is approximately 200 μK. The linear Paul

trap structure in this study includes four parallel radio-frequency electrode rods, two end electrodes, and several fixtures [25]. The diameter of the radio-frequency electrode rods is approximately 3 mm, the length is 10 cm, and the rod spacing is 15 mm. The end electrodes are ring-shaped with an inner diameter of 10 mm. An axial gap of approximately 1 ° is provided to break the ring, which avoids the generation of eddy current electric fields. The axial center-to-center distance between the two end electrodes is 10 cm. During operation, one pair of rods in the quadrupole is connected to the radio-frequency voltage $+U_{\mathrm{RF}}$, while the other pair is connected to the anti-phase radio-frequency voltage $-U_{\mathrm{RF}}$. The two end electrodes are loaded with the same positive voltage to achieve ion trapping and extraction. The depth of the linear Paul trap is approximately 0.7 eV, the maximum number of ions that can be trapped is approximately 10^6, and the ion temperature ranges between 10^3 and 10^4 K. Ions are prepared via two-step photoionization of cold rubidium atoms using cooling light and continuous semiconductor ionization light (wavelength λ_{ion} is 478.8 nm). The initial temperature is determined by energy and momentum conservation and is close to the atomic temperature.

The spatial orientation of an ion trap is typically defined by its axis of symmetry (axial direction, denoted as *z*, which is the direction of the quadrupole rods) and the plane perpendicular to it (radial direction, the plane perpendicular to the quadrupole rods). The radial position is characterized by the planar vector $\boldsymbol{r} = (x, y)$, whose components *x* and *y* point to two mutually perpendicular radial directions. The expression for the electric potential near the center of the trap is given by[26,27]

$$\begin{aligned} \Phi(x,y,z,t) \approx \quad & [U_{\mathrm{DC}} + U_{\mathrm{RF}}\cos(\Omega_{\mathrm{RF}}t)]\frac{x^2-y^2}{r_0^2} \\ & + \frac{\kappa U_{\mathrm{END}}}{z_0^2}\left(z^2 - \frac{x^2+y^2}{2}\right), \end{aligned} \tag{1}$$

Here, U_{DC} denotes the amplitude of the DC bias for the RF signal, U_{END} represents the DC potential applied to the end electrodes, U_{RF} indicates the peak voltage of the confining RF field (i.e., its amplitude), and Ω_{RF} is the angular frequency of the confining RF field. In all experiments presented in this study, U_{DC} and U_{END} are fixed at 0 V and 90.0 V, respectively. The peak voltage and angular frequency of the confining RF field are specified in the captions of the corresponding result figures. The parameter r_0 = 9.1 mm represents the minimum distance from the quadrupole rods to the central axis of the ion trap, while z_0 = 50 mm denotes the minimum distance from the end electrodes to the trap center. The geometric factor $\kappa = 0.065$ depends on the trap geometry and was determined through simulations using COMSOL Multiphysics software.

The radial and axial trap depths of the linear Paul trap in this study are given by[28]

$$\begin{aligned} D_r &= \frac{e^2 U_{\mathrm{RF}}^2}{m r_0^2 \Omega_{\mathrm{RF}}^2} - \frac{e\kappa U_{\mathrm{END}} r_0^2}{2 z_0^2} \propto \frac{U_{\mathrm{RF}}^2}{\Omega_{\mathrm{RF}}^2}, \\ D_z &= \kappa e U_{\mathrm{END}}, \end{aligned} \tag{2}$$

Here, e denotes the ionic charge, and m represents the ion mass.
In such a potential field, the dynamic behavior of single-component ions or weakly coupled multi-component ions is described by the Mathieu equation, characterized by parameters a_u and q_u[29,30], as shown in Eq. (3). The parameter q_u is directly related to the frequency Ω_{RF} and amplitude U_{RF} of the applied radiofrequency field.

$$\frac{\mathrm{d}^2 u(\tau)}{\mathrm{d}\tau^2} + (a_u - 2q_u \cos 2\tau) u(\tau) = 0, u = x, y, z, \tag{3}$$

$\tau = \Omega_{\mathrm{RF}} t/2$. Here, a_u and q_u denote the Mathieu parameters.

$$q_x = -q_y = \frac{4eU_{\mathrm{RF}}}{m r_0^2 \Omega_{\mathrm{RF}}^2}, q_z = 0, \tag{4}$$

$$a_x = a_y = -\frac{a_z}{2} = \frac{-4e\kappa U_{\mathrm{end}}}{m z_0^2 \Omega_{\mathrm{RF}}^2}. \tag{5}$$

When the direct current bias of the ion trap radio frequency signal is $U_{\mathrm{DC}} = 0$, the first stability region begins at $q_x = 0$ and ends at $q_x = 0.908$. The radial macromotion frequency of the ions is[9,23]

$$\begin{aligned} \omega_r &= \frac{\Omega_{\mathrm{RF}}}{2} \sqrt{(-\frac{4eU_{\mathrm{RF}}}{m r_0^2 \Omega_{\mathrm{RF}}^2})^2/2 - \frac{8\kappa e U_{\mathrm{END}}}{m z_0^2 \Omega_{\mathrm{RF}}^2}} \\ &\approx \frac{\sqrt{2} eU_{\mathrm{RF}}}{m r_0^2 \Omega_{\mathrm{RF}}}. \end{aligned} \tag{6}$$

In the expression for the radial macro-motion frequency of this ion, the second term under the square root is negligible. Thus, the approximation $\omega_r \approx \frac{\sqrt{2} eU_{\mathrm{RF}}}{m r_0^2 \Omega_{\mathrm{RF}}}$ applies. The axial macro-motion frequency of the ion is given by[9,23]

$$\omega_z = \sqrt{\frac{2\kappa e U_{\mathrm{END}}}{m z_0^2}}. \tag{7}$$

In the experimental setup described in this paper, the axial secular frequency of the ions, ω_z, is approximately 10 kHz. The radial secular frequency, ω_r, depends on the trapping radiofrequency (RF) field parameters $\Omega_{\mathrm{RF}}, U_{\mathrm{RF}}$ and is approximately inversely proportional to the ion mass, as shown in Eq. (6).

In multi-component ion systems, achieving precise identification and manipulation of specific ion species represents a core challenge for applications such as mass spectrometry and reaction process control. Various ion manipulation techniques exist, among which methods based on resonant excitation have attracted significant attention due to their excellent mass selectivity. These methods primarily operate through two distinct physical mechanisms: displacement driving and parametric resonance [31]. Displacement driving applies an independent oscillating electric field to translate the entire potential well, thereby driving forced ion vibration. In contrast, parametric resonance periodically modulates the parameters of the trapping potential well itself (such as the RF amplitude, which corresponds to the well "stiffness") [32]. When the modulation frequency matches an integer multiple of the ion secular frequency, the ion's motion amplitude grows exponentially until the ion escapes the trap; this effect enables mass-selective ion ejection. Studies in Ref. [31] indicate that the linewidth of parametric resonance is significantly narrower than that of displacement driving.

The frequency of the trapping RF field is typically much higher than the ion secular frequency. Its primary role is to provide a dynamic confining potential without directly exciting ion resonances. However, when the RF field frequency is exactly an integer multiple (with a minimum of two times) of the ion secular frequency, it directly excites parametric resonance, causing ion heating and ejection. In this case, the corresponding Mathieu parameter q_x equals $\sqrt{2}$, as demonstrated below:

$$\omega_r \approx \frac{\Omega_{\mathrm{RF}}}{2}\sqrt{\frac{1}{2}q_x^2} = \frac{\Omega_{\mathrm{RF}}}{2} \rightarrow q_x = \sqrt{2}. \tag{8}$$

As previously mentioned, when $q_x > 0.908$, ions cannot be stably trapped. Accordingly, no experimental work has yet reported direct excitation of parametric resonance by the trapping radio-frequency field. Existing experiments achieve this by frequency-modulating the trapping radiofrequency field, with the modulation frequency equal to the parametric resonance frequency of the ions [31,33].

Each experimental cycle is illustrated in Figure 1. First, the magneto-optical trap is activated to load cold atoms until stability is achieved. Subsequently, while maintaining the magneto-optical trap, the ionization laser and ion trap are simultaneously turned on to generate and trap charged particles. After continuous photoionization of the cold atoms for a duration T_{reac}, the magneto-optical trap, ionization laser, and the end cap electrode near the microchannel plate (Endcap2 in Figure 1) are simultaneously switched off. The trapping radiofrequency field and the end cap electrode distant from the microchannel plate (Endcap1 in Figure 1) remain active. Under these conditions, ions experience an electric field directed toward the microchannel plate and are guided axially toward it. Upon impacting the microchannel plate, the signal is amplified via

electron multiplication, thereby yielding the time-of-flight mass spectrometry signal.

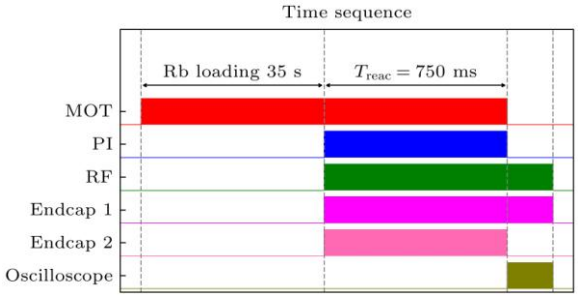

Fig. 1 Time sequence. Load the magneto-optical trap for 35 s until the cold atoms are saturated; then turn on the 478.8 nm ionization light (PI) and the ion trap. Keep the magneto-optical trap, ionization light, and ion trap on together for a duration of T_{reac}; then turn off the magneto-optical trap, ionization light, and the endcap electrode near the microchannel plate (Endcap2), and export the ion time-of-flight mass spectrum. In all experiments, $T_{\mathrm{reac}} = 750$ ms.

In a typical time-of-flight mass spectrum, two asymmetric peaks are observable. The peak with a shorter flight time (Peak 1) exhibits higher intensity and a narrower profile, whereas the peak with a longer flight time (Peak 2) shows lower intensity and a broader profile. Our previous work [34] indicates that Peak 1 and Peak 2 correspond to atomic ions $^{87}Rb^{+}$ and rubidium molecular ions $^{87}Rb_N^{+}(N = 2,3,\cdots)$, respectively.

The formation of rubidium molecular ions $^{87}Rb_N^{+}(N = 2,3,\cdots)$ is attributed to the following mechanism [34]: In the ion-atom hybrid trap, the magneto-optical trap continuously generates cold atoms. The photoionization of these cold atoms produces a high ion density that spatially overlaps with the atomic cloud. Consequently, the large ion-atom collision cross-section ensures that reactive collisions occur over sufficiently short distances. More importantly, the ion trap effectively stores the charged reaction products, enabling subsequent cascade reactions (such as $^{87}Rb^{+}+{}^{87}Rb \rightarrow {}^{87}Rb_2^{+}$ and $^{87}Rb_2^{+}+{}^{87}Rb \rightarrow {}^{87}Rb_3^{+}$) to generate polyatomic clusters [34]. To extract intensity and width information from the peaks, we fitted the time-of-flight mass spectra using a Gumbel-type extreme value distribution function, based on the work of Liang Weichen et al.[35].

Experimental errors primarily arise from the following factors: an uncertainty of 1%—5% in the measurement of ionization light intensity, and an uncertainty of 1 MHz in the measurement of laser frequency/wavelength for the cooling/trapping, repumping, and detection/imaging lasers. This uncertainty increases to 600 MHz when λ_{ion} = 478.8 nm. In this study, experimental errors are dominated by statistical errors. Each data point represents the average of three repeated measurements, with the error defined by the standard deviation of the dataset.

3 Results and Discussion

By independently adjusting the frequency and amplitude of the radiofrequency field in the linear Paul trap, we measured the time-of-flight mass spectra obtained under a combined action time of 750 ms for the magneto-optical trap, ionization light, and linear Paul trap. We also determined the corresponding total ion counts, as shown in Figure 2. The experiment reveals that the two curves describing the total ion count as a function of q_x ($^{87}Rb^+$) largely overlap. This observation aligns with the expected behavior described by the Mathieu equation in Eq. (3): the motion of ions in the trap is jointly determined by the Mathieu parameters a_u and q_u ($u = x, y, z$). Although both a_u and q_u change when adjusting the radiofrequency field frequency or amplitude, the condition $a_u \ll q_u$ typically holds. Thus, the actual impact of changes in a_u is negligible, and the stability of ion motion depends primarily on the values of q_x (and q_y). Therefore, when q_x remains constant, the ion motion state should remain essentially consistent.

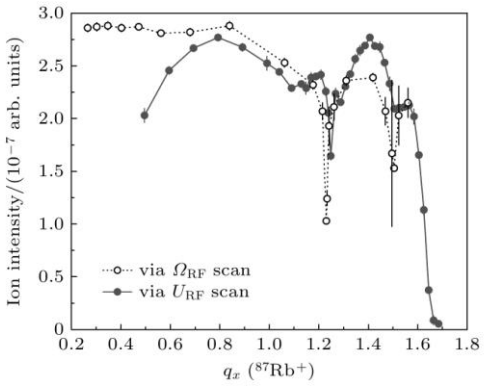

Fig. 2 Total ion number as a function of the Mathieu parameter q_x for atomic ions $^{87}Rb^+$. The total ion signal was obtained from time-of-flight mass spectra. Each data point represents the average of three measurements. Solid dots: the $q_x(^{87}Rb^+)$ parameter was varied by scanning the frequency of the trapping RF field while its peak RF voltage was fixed at 140.0 V. Hollow dots: the $q_x(^{87}Rb^+)$ parameter was varied by scanning the peak RF voltage of the trapping RF field while its frequency was fixed at 350.0 kHz.

Figure 2 illustrates the variation in total ion count as a function of $q_x(^{87}Rb^+)$. Two extremely narrow minima appear near $q_x(^{87}Rb^+) = \sqrt{2}$. In other $q_x(^{87}Rb^+)$ intervals, the total ion count remains at a saturated level. Notably, the total ion count does not decrease significantly even in the theoretically unstable region where $q_x(^{87}Rb^+) > 0.908$. However, in the interval where $q_x(^{87}Rb^+) < 0.7$, the total ion count obtained by scanning the RF field amplitude is significantly lower than that obtained by scanning the frequency under the same $q_x(^{87}Rb^+)$ conditions.

The following analysis addresses three aspects. First, we examine the difference in total

ion count between the two scanning methods when $q_x(^{87}\mathrm{Rb}^+) < 0.7$. Second, we confirm the experimental observation that rubidium ions $^{87}\mathrm{Rb}^+$ remain stable when $q_x(^{87}\mathrm{Rb}^+) > 0.908$. Finally, we reveal the physical mechanism behind the extremely narrow minima in total ion count at specific $q_x(^{87}\mathrm{Rb}^+)$ values.

3.1 Influence of Ion Trap Depth on Trapped Ion Count

As shown in Figure 2, the ion count decreases significantly when $q_x(^{87}\mathrm{Rb}^+) < 0.7$ during RF field amplitude scanning. In contrast, the ion count remains largely unchanged in this region during RF field frequency scanning. This phenomenon is closely related to the trap depth of the ion trap. Specifically, the radial trap depth D_r of a linear Paul trap depends on the frequency and amplitude of the RF field. As shown in Equation (2), $D_r \propto U_{\mathrm{RF}}^2/\Omega_{\mathrm{RF}}^2$. The axial trap depth D_z, however, is independent of the RF field frequency and amplitude. Figure 3 presents the curve of relative radial trap depth $U_{\mathrm{RF}}^2/\Omega_{\mathrm{RF}}^2$ as a function of $q_x(^{87}\mathrm{Rb}^+)$. In the region where $q_x(^{87}\mathrm{Rb}^+) < 0.7$, the radial trap depth corresponding to RF field amplitude scanning is significantly lower than that for frequency scanning. This difference in trap depth results in a significantly lower total number of trapped ions during amplitude scanning compared to frequency scanning within this parameter range.

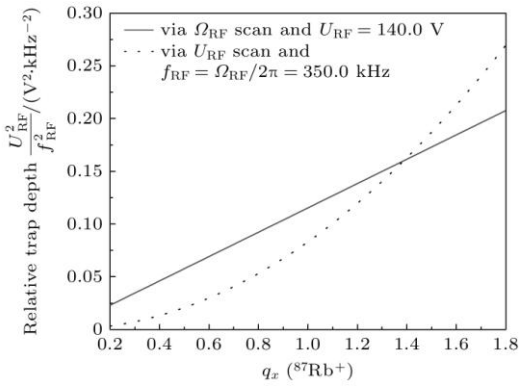

Fig. 3 The radial relative trap depth of our linear Paul Trap as a function of the Mathieu parameter q_x for atomic ions $^{87}\mathrm{Rb}^+$. Solid line: the $q_x(^{87}\mathrm{Rb}^+)$ parameter was varied by scanning the RF frequency with the peak RF voltage fixed at 140.0 V. Dotted line: the $q_x(^{87}\mathrm{Rb}^+)$ parameter was varied by scanning the peak RF voltage with the frequency fixed at 350.0 kHz.

3.2 Extended Stability Region: $q_x(^{87}\mathrm{Rb}^+) > 0.908$

As shown in Figure 2, the total ion count does not exhibit a significant decline in the theoretically unstable region where $q_x(^{87}\mathrm{Rb}^+) > 0.908$. To verify this phenomenon, we analyzed the relationship between ion intensity and storage time. Here, storage time refers to the duration T_{Hold} during which the ion trap remains active after the ionization light and magneto-optical trap are switched off, following a joint interaction period

T_{reac}. We then measured the time-of-flight mass spectrum to obtain ion count data. Figure 4 illustrates the intensity trends for atomic and molecular ions within a storage time of 0—250 ms, a range where time-of-flight mass spectrometry clearly resolves atomic and molecular ion peaks. These measurements were conducted with a trapping RF field frequency of 346.0 kHz and an amplitude of 140.0 V ($q_x(^{87}\mathrm{Rb}^+)\approx\sqrt{2}$). The atomic ion intensity remains essentially constant during this storage period, whereas the molecular ion intensity decays significantly over time. The decrease in molecular ion intensity primarily results from losses due to the limited confinement capacity of the ion trap and dissociation processes. In contrast, the approximately constant atomic ion intensity reflects a dynamic equilibrium between two competing processes: ion loss from the trap and the generation of atomic ions via molecular ion dissociation. This result indicates that atomic ions possess high stability within the trap. If the intrinsic loss rate of atomic ions were high, their signal intensity would decrease with increasing storage time, even with continuous contributions from molecular ion dissociation. The observed steady-state behavior in the experiment thus supports the conclusion that atomic ions can remain stable under extended q_x conditions.

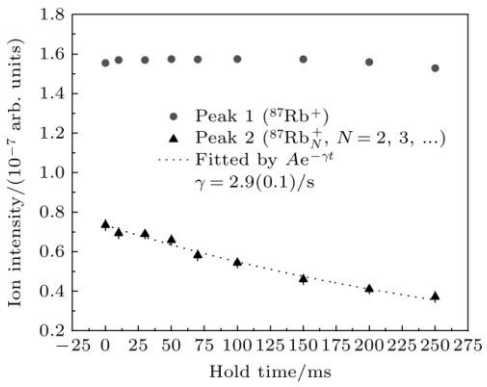

Fig. 4 Signal intensities of atomic and molecular ions as a function of storage time. The dotted line is an exponential fit to the molecular ion data. Experimental conditions: trapping RF frequency 346.0 kHz, peak RF voltage 140.0 V ($q_x(^{87}\mathrm{Rb}^+) = 1.52, \omega_r(^{87}\mathrm{Rb}^+)/2\pi = 185.5$ kHz). Each data point is the average of three measurements.

To further quantitatively assess the stability of atomic ions, this paper presents an upper-bound analysis of the ion loss rate. We modeled the experiment and derived the rate equations for atomic ions, molecular ions, and the total ion count as follows[34]:

$$\begin{aligned} \frac{\mathrm{d}I_{\mathrm{m}}}{\mathrm{d}t} &= -(k_{\mathrm{d}}+\gamma_{\mathrm{m}})I_{\mathrm{m}}, \\ \frac{\mathrm{d}I_{\mathrm{a}}}{\mathrm{d}t} &= k_{\mathrm{d}}I_{\mathrm{m}}-\gamma_{\mathrm{a}}I_{\mathrm{a}}, \\ \frac{\mathrm{d}(I_{\mathrm{a}}+I_{\mathrm{m}})}{\mathrm{d}t} &= -\gamma_{\mathrm{m}}I_{\mathrm{m}}-\gamma_{\mathrm{a}}I_{\mathrm{a}}, \end{aligned} \tag{9}$$

Here, $I_{\mathrm{m}}, I_{\mathrm{a}}$ denote the numbers of rubidium molecular ions and rubidium atomic ions,

respectively; k_{d} represents the rate at which molecular ions dissociate into atomic ions; and $\gamma_{\mathrm{m}}, \gamma_{\mathrm{a}}$ indicate the loss rates of rubidium molecular ions and rubidium atomic ions in the trap, respectively.

The total ion number decay observed in the experiment reflects the loss rate of all ions in the trap (excluding dissociation). As shown in Figure 5, this decay approximates an exponential function with a corresponding loss rate of 0.76(0.03)/s and a lifetime of approximately 1.3 s. To estimate the upper bound of the atomic ion loss rate, we adopt a conservative assumption that all observed total ion loss originates from atomic ions, ignoring the loss rate of molecular ions in the trap. Under this worst-case scenario, the lower bound for the trapping lifetime of atomic ions is derived to be approximately 1.3 s. This lifetime is significantly longer than the characteristic decay time of molecular ions (approximately 0.34 s, see Figure 4). Thus, we can confidently assert that atomic ions exhibit high stability under the extended q-value conditions. This conservative estimate provides robust quantitative support to our qualitative observations.

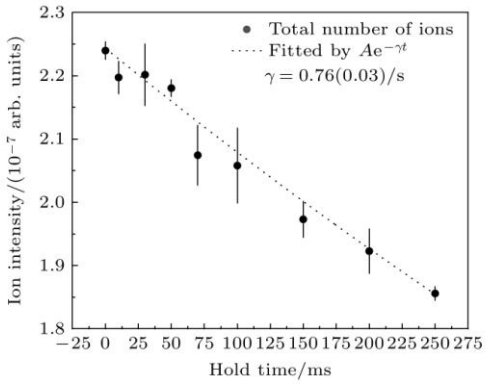

Fig. 5 Signal intensities of total ions as a function of storage time. The dotted line is an exponential fit to the molecular ion data. Experimental conditions: trapping RF frequency 346.0 kHz, peak RF voltage 140.0 V ($q_x(^{87}\mathrm{Rb}^+) = 1.52, \omega_r(^{87}\mathrm{Rb}^+)/2\pi = 185.5$ kHz). Each data point is the average of three measurements.

The results shown in Figure 2 reveal that the total ion count exhibits a non-monotonic structure with two minima near $q_x(^{87}\mathrm{Rb}^+) \approx \sqrt{2}$. This complex phenomenon cannot be predicted or explained by single-particle theories or weakly coupled multi-component molecular theories based on independent Mathieu equations. The results clearly indicate that collective interactions dominate the dynamic behavior in strongly coupled, multi-component systems near the parameter instability boundary, exceeding the descriptive scope of existing simplified models.

We initially attribute the stable existence of atomic ions at $q_x(^{87}\mathrm{Rb}^+) \approx \sqrt{2}$ to the synergistic confinement effect of component ions. When the system consists of rubidium ion clusters $^{87}\mathrm{Rb}_N^+(N = 1,2,\cdots)$ with mass-to-charge ratios forming an arithmetic progression, the radial macromotion frequencies of the components in the

linear Paul trap approximately form a harmonic sequence ($\approx 1: 1/2: 1/3 \cdots$), as shown in Equation (6). Under strong Coulomb coupling, these multi-component ions, whose macromotion frequencies constitute a subharmonic sequence, collectively expand the stability region of atomic ions through collective interactions.

However, this qualitative mechanism is insufficient to quantitatively characterize the fine double-peak structure in the loss curve. Revealing the underlying microscopic physics requires full-scale numerical simulations based on multi-ion trapping dynamic equations. This presents significant challenges because nonlinearities, many-body correlations, and couplings of multi-component collective modes are highly pronounced in the strongly unstable region where $q_x \approx \sqrt{2}$. Therefore, developing specialized numerical methods capable of accurately handling such strongly coupled many-body instabilities is not only key to explaining the experimental results but also represents an independent and important future theoretical endeavor to deepen the understanding of collective dynamics in multi-component ion traps.

3.3 Parametric Resonance of Rubidium Atomic Ions Excited by Trapping RF Fields

We now discuss the causes of the minima in the total ion count shown in Figure 2. First, no atomic ions are present at the minima. We compared the time-of-flight mass spectra at the two minima (336.0 kHz and 371.0 kHz) and at the intermediate frequency point (346.0 kHz) from the frequency sweep experiment, as shown in Figure 6. The time-of-flight mass spectrum at an RF field frequency of 346.0 kHz ($q_x(^{87}\mathrm{Rb}^+) \approx \sqrt{2}$) displays two ion signal peaks. In contrast, at an RF field frequency of 336.0 kHz ($q_x(^{87}\mathrm{Rb}^+) = 1.5$), the first peak disappears while the position of the second peak remains unchanged compared to the spectrum at 346.0 kHz. Similarly, comparing the time-of-flight mass spectrum at an ion trap RF frequency of 371.0 kHz ($q_x(^{87}\mathrm{Rb}^+) = 1.2$) with that at 346.0 kHz reveals the same phenomenon: the first peak disappears, and the position of the second peak remains essentially unchanged. We also compared the time-of-flight mass spectra from the amplitude sweep experiment near the two minima (126.0 V and 152.0 V) and at an amplitude of 142.0 V ($q_x(^{87}\mathrm{Rb}^+) \approx \sqrt{2}$), as shown in Figure 7. Similarly, the time-of-flight mass spectra at the minima exhibit only the second peak, whereas the spectrum at an ion trap RF amplitude of 142.0 V displays two ion signal peaks. This confirms the absence of atomic ions at the minima.

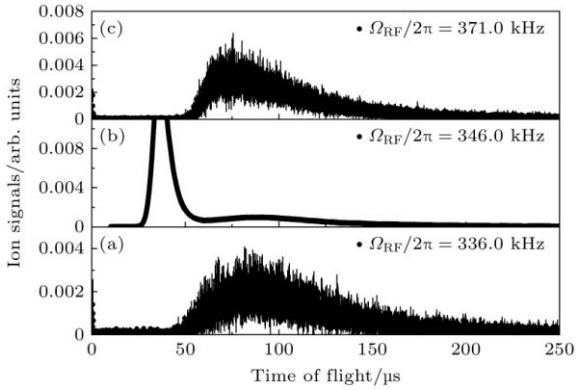

Fig. 6 Time-of-flight mass spectra measured at different trapping RF frequencies with a fixed peak RF voltage of 140.0 V: (a) 336.0 kHz ($q_x(^{87}\mathrm{Rb}^+) = 1.61, \omega_r(^{87}\mathrm{Rb}^+) = 191.3$ kHz); (b) 346.0 kHz ($q_x(^{87}\mathrm{Rb}^+) = 1.52, \omega_r(^{87}\mathrm{Rb}^+) = 185.5$ kHz); (c) 371.0 kHz ($q_x(^{87}\mathrm{Rb}^+) = 1.31, \omega_r(^{87}\mathrm{Rb}^+) = 173.0$ kHz). Each spectrum is the average of three measurements.

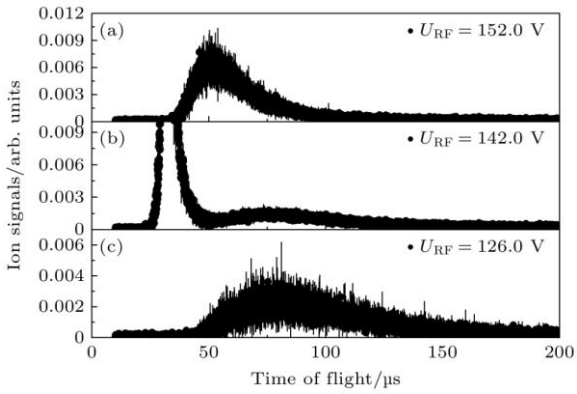

Fig. 7 Time-of-flight mass spectra measured at a fixed trapping RF frequency of 350.0 kHz with different peak RF voltages: (a) 152.0 V ($q_x(^{87}\mathrm{Rb}^+) = 1.61, \omega_r(^{87}\mathrm{Rb}^+)/2\pi = 199.3$ kHz); (b) 142.0 V ($q_x(^{87}\mathrm{Rb}^+) = 1.51, \omega_r(^{87}\mathrm{Rb}^+) = 186.9$ kHz); (c) 126.0 V ($q_x(^{87}\mathrm{Rb}^+) = 1.33, \omega_r(^{87}\mathrm{Rb}^+)/2\pi = 164.6$ kHz). Each spectrum is the average of three measurements.

The phenomenon of two minima in the total ion count near $q_x(^{87}\mathrm{Rb}^+) = \sqrt{2}$ arises from parametric resonance of atomic ions excited by the trapping radiofrequency (RF) field of the linear Paul trap, which causes the atomic ions to escape. Specifically, first, as previously stated, our experiments demonstrate that multi-component ions can remain stable in the region where $q_x > 0.908$. Second, as shown in Eq. (8), when $q_x = \sqrt{2}$, the RF field frequency is twice the radial macromotion frequency of the ions. This condition excites parametric resonance in these ions, causing them to escape the ion trap, while molecular ions remain effectively confined. Consequently, the total ion count decreases, and the structure of the time-of-flight mass spectrometry peaks changes.

We note that the appearance of two minima is closely related to the nonlinearity of the trap potential caused by the co-trapping of different ion species. This nonlinear effect

leads to combination frequency coupling in the transverse motion direction, thereby inducing two separate resonance dips near this q value. Taking the frequency scan experiment as an example, when the trapping RF field frequency Ω is 346.0 kHz, it is exactly twice the radial macromotion frequency ω_r of the rubidium atomic ions, while the axial macromotion frequency ω_z of the rubidium atomic ions is 10 kHz. In this case, parametric resonance occurs within the trapping frequency range near 346.0 kHz. Due to trap imperfections or space charge effects, oscillation modes in different directions couple, generating higher-order combination frequencies $2\omega_r \pm \omega_z$. These correspond roughly to the centers of the two observed dips at 336.0 kHz and 371.0 kHz.

We fitted the four total ion count dips from the frequency scan and amplitude scan experiments to obtain the widths of the minima. Figures 8(a) and 8(b) show the variation of the total ion signal with frequency when the trapping RF field amplitude is fixed at 140.0 V. Two distinct minima are observed, with corresponding frequencies of 371.2(0.2) kHz and 336.3(0.4) kHz, and full widths at half maximum (FWHM) of 2.2(0.4) kHz and 4.1(1.8) kHz, respectively. Comparing these bandwidths with those obtained by implementing parametric resonance through frequency modulation of the trapping RF field, Reference [31] reported a bandwidth of 1 kHz, while Reference [33] achieved a bandwidth of 240 Hz by combining pre-excitation and parametric resonance. The bandwidth in this study is comparable in magnitude to the results in Reference [31], demonstrating the selective manipulation and precise removal of specific ions via parametric resonance. Similarly, Figures 8(c) and 8(d) illustrate the relationship between the total ion signal and amplitude when the trapping RF field frequency is fixed at 350.0 kHz. Under these conditions, two minima are also observed. The minimum near 152.0 V is shallow and exhibits an asymmetric line shape, making it impossible to obtain a reliable FWHM via Lorentzian fitting. In contrast, for the minimum near 127.3(0.2) V, the FWHM obtained through Lorentzian fitting is 2.5(0.8) V. Notably, the measurement error of the total ion signal is large at the minimum near 336.3 kHz, which may indicate that this resonance point itself is unstable.

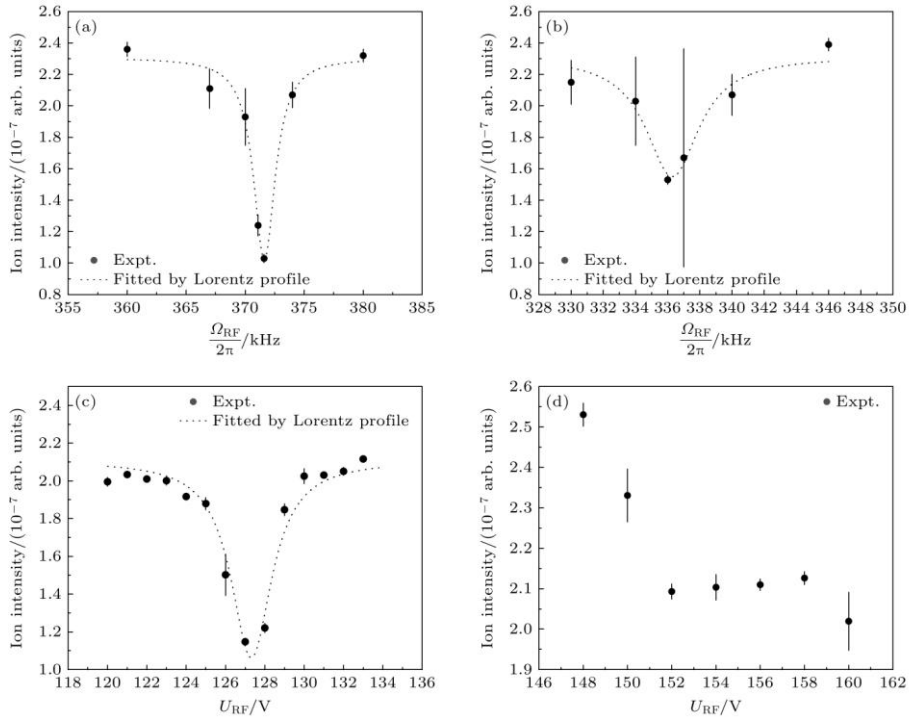

Fig. 8 Widths of the four ion number binima in the sweep frequency and sweep peak RF voltage experiments: (a) The minimum of ion number near 371.0 kHz in the sweep frequency experiment; (b) the minimum of ion number near 336.0 kHz in the sweep frequency experiment; (c) the minimum of ion number near 127.0 V in the sweep peak RF voltage experiment; (d) the minimum of ion number near 152.0 V in the sweep peak RF voltage experiment. Each data point is the average of three measurements.

4 Conclusion

This study experimentally investigated the confinement characteristics of a multi-component system composed of rubidium ion clusters $^{87}Rb_N^+(N = 1,2,\cdots)$ with mass-to-charge ratios forming an arithmetic progression in a linear Paul trap. Based on an ion-atom hybrid trap, we prepared rubidium ion clusters with mass-to-charge ratios in an arithmetic progression via continuous photoionization. We altered the Mathieu parameters by scanning the frequency or amplitude of the confining radiofrequency (RF) field and measured the corresponding time-of-flight mass spectra to obtain ion count information. Experimental observations indicate that $^{87}Rb^+$ atomic ions can maintain stable confinement within the theoretically unstable region for single-component ions where the Mathieu parameter $q_x > 0.908$. Furthermore, their lifetime exceeds that of cluster molecular ions (see Figures 2, 4, and 5). Single-component ion theory cannot explain this phenomenon. We attribute it to the sympathetic confinement effect, whereby multi-component ions with subharmonic frequency relationships collectively expand the actual stable region of the trap through collective interactions.

The expansion of the stable region enables exploration within zones traditionally considered forbidden by theory. Based on this, we observed two sharp minima in the total ion signal near $q_x(^{87}\mathrm{Rb}^+) \approx \sqrt{2}$ (see Figure 2). Analysis suggests that this phenomenon stems from parametric resonance excited by the confining RF field on the atomic ions. Under the nonlinear coupling of multi-component ions, the frequencies of ionic motional modes along different directions become coupled. This correlation generates two parametric resonance frequencies, resulting in double sharp minima in the total ion count near $q_x(^{87}\mathrm{Rb}^+) \approx \sqrt{2}$.

This work deepens the understanding of multi-component ion dynamics in ion traps. It opens new avenues for achieving selective ion manipulation in quantum systems and studying multi-component plasma physics. Future research may focus on the following directions: conducting molecular dynamics simulations that include ion-ion interactions to quantitatively reveal the microscopic mechanisms of the aforementioned collective effects. Additionally, the sympathetic confinement effect revealed in this study provides new technical insights for the efficient confinement and manipulation of ions with high mass-to-charge ratios.

References

[1] Tomza M, Jachymski K, Gerritsma R, Negretti A, Calarco T, Idziaszek Z, Julienne P S 2019 *Rev. Mod. Phys.* **91** 035001

[2] Deiß M, Willitsch S, Hecker Denschlag J 2024 *Nat. Phys.* **20** 713

[3] Karman T, Tomza M, Pérez-Ríos J 2024 *Nat. Phys.* **20** 722

[4] Barrett M, Arnold K, Safronova M 2019 *Phys. Rev. A* **100** 043418

[5] Wolf F 2024 *Phys. Rev. Lett.* **132** 083202

[6] Steinel M, Shao H, Filzinger M, Lipphardt B, Brinkmann M, Didier A, Mehlstäubler T, Lindvall T, Peik E, Huntemann N 2023 *Phys. Rev. Lett.* **131** 083002

[7] Ma Z X, Zhang B L, Huang Y, Gao K L, Guan H 2025 *Acta Phys. Sin.* **74** 094204

[8] Zhang H S, Zhou Y Z, Shen Y, Zou H X 2023 *Acta Phys. Sin.* **72** 013701

[9] Wang C X, He R, Li R R, Chen Y, Fang D, Cui J M, Huang Y F, Li C F, Guo G C 2022 *Acta Phys. Sin.* **71** 133701

[10] Zawierucha M J, Rehmert T, Keller J, Mehlstäubler T E, Schmidt P O, Wolf F 2024 *Phys. Rev. A* **110** 013107

[11] Guo S A, Wu Y K, Ye J, et al. 2024 *Nature* **630** 613

[12] Paul A, Noel C 2024 *Phys. Rev. Appl.* **22** 044033

[13] Yang X Y, Lin Z D, Mu S Y, Wu W, Wu C W, Xie Y, Chen P X 2024 *Chin. Phys. Lett.* **41** 113702
[14] Wu Y K, Duan L M 2024 *Sci. Bull.* **69** 3480
[15] Zalivako I V, Semenin N V, Zhadnov N O, et al. 2025 *Phys. Usp.* **68** 552
[16] Caplan M 2020 *Phys. Rev. E* **101** 023201
[17] Caplan M, Yaacoub D 2024 *Phys. Rev. Lett.* **133** 135301
[18] Kozhberov A 2024 *Phys. Rev. E* **110** 045206
[19] Huang Y, Zhang B, Zeng M, Hao Y, Ma Z, Zhang H, Guan H, Chen Z, Wang M, Gao K 2022 *Phys. Rev. Appl.* **17** 034041
[20] Sosnova K, Carter A, Monroe C 2021 *Phys. Rev. A* **103** 012610
[21] Mao Z C, Xu Y Z, Mei Q X, et al. 2021 *Phys. Rev. Lett.* **127** 143201
[22] Tanaka U, Masuda K, Akimoto Y, Koda K, Ibaraki Y, Urabe S 2012 *Appl. Phys. B* **107** 907
[23] Li H X, Li M, Zhang Q Y, Tong X 2019 *Chin. Phys. Lett.* **36** 073701
[24] Ravi K, Lee S, Sharma A, Werth G, Rangwala S 2012 *Nat. Commun.* **3** 1
[25] Lv S F, Jia F D, Liu J Y, Xu X Y, Xue P, Zhong Z P 2017 *Chin. Phys. Lett.* **34** 013401
[26] Drakoudis A, Söllner M, Werth G 2006 *Int. J. Mass Spectrom.* **252** 61
[27] Goodman D S, Sivarajah I, Wells J E, Narducci F A, Smith W W 2012 *Phys. Rev. A* **86** 033408
[28] Raizen M, Gilligan J, Bergquist J, Itano W M, Wineland D J 1992 *J. Mod. Opt.* **39** 233
[29] Keller J, Partner H L, Burgermeister T, Mehlstäubler T 2015 *J. Appl. Phys.* **118** 104501
[30] Sivarajah I, Goodman D, Wells J, Narducci F, Smith W 2012 *Phys. Rev. A* **86** 063419
[31] Schmidt J, Honig D, Weckesser P, Thielemann F, Schaetz T, Karpa L 2020 *Appl. Phys. B* **126** 176
[32] Landau L D, Lifshits E M 1960 *Mechanics*, **1** (CUP Archive
[33] Yu N, Dehmelt H, Nagourney W 1993 *J. Appl. Phys.* **73** 8650
[34] Liang W C, Jia F D, Wang F, Zhang X, Wang Y H, Qian J Y, Hu X Q, Wu Y, Wang J G, Xue P, Zhong Z P 2024 arXiv.2303.10360 [physics.atom-ph]
[35] Liang W C, Wang Y H, Zhang X, Wang F, Jia F D, Xue P, Zhong Z P 2023 *Acta Phys. Sin.* **72** 093401